nature energy

ARTICLES

PUBLISHED: 20 MARCH 2017 | VOLUME: 2 | ARTICLE NUMBER: 17032

Silicon heterojunction solar cell with interdigitated back contacts for a photoconversion efficiency over 26%

Kunta Yoshikawa*, Hayato Kawasaki, Wataru Yoshida, Toru Irie, Katsunori Konishi, Kunihiro Nakano, Toshihiko Uto, Daisuke Adachi, Masanori Kanematsu, Hisashi Uzu and Kenji Yamamoto

Improving the photoconversion efficiency of silicon solar cells is crucial to further the deployment of renewable electricity. Essential device properties such as lifetime, series resistance and optical properties must be improved simultaneously to reduce recombination, resistive and optical losses. Here, we use industrially compatible processes to fabricate large-area silicon solar cells combining interdigitated back contacts and an amorphous silicon/crystalline silicon heterojunction. The photoconversion efficiency is over 26% with a 180.4 cm^2 designated area, which is an improvement of 2.7% relative to the previous record efficiency of 25.6%. The cell was analysed to characterize lifetime, quantum efficiency, and series resistance, which are essential elements for conversion efficiency. Finally, a loss analysis pinpoints a path to approach the theoretical conversion efficiency limit of Si solar cells, 29.1%.

Today's energy production strongly depends on fossil fuels such as oil, natural gas and coal with limited minable years[1], while the world energy demand is predicted to increase in the future[2]. As a renewable energy source, solar cells are one of the most widely used technologies utilizing sunlight to generate electricity, demonstrated with strong growth of photovoltaic module installation[3], and grid parity has already been achieved in many countries[4]. According to several scenarios, by the year 2050, photovoltaic electricity should cover more than a 20% share of the global primary energy demands[5]. Indeed, the performance of industrial solar cells has improved continuously together with the cost and reliability[6]. Such progress indicates the remarkable maturation of the technology.

Silicon has a nearly optimum bandgap for sunlight absorption and silicon solar cells reach a high photoconversion efficiency due to the good material quality and widespread technological know-how. Moreover, Si solar cells have several strong advantages essential for photovoltaics, such as abundant raw material supply, low toxicity, low cost and scalable technologies for cell and module fabrication. These advantages are at the origin of the sharp increase in the number of photovoltaic installations in the world, and most probably the same trend will continue in the future. Improving the efficiency of Si solar cells is key to further reduce area-related costs and to ascertain the position of photovoltaics as a renewable source of electricity.

In the last years, several high conversion efficiencies have been reported[7,8]. There are mainly two technologies responsible for this progress: first, the passivated contact technology including heterojunctions (HJ); and second, the interdigitated back contact (IBC) technology. The HJ technology using an amorphous Si (a-Si) layer to passivate the crystalline Si (c-Si) surface was first reported by Sanyo (now Panasonic) and following work was reported in 2000[9]. The very origin of the IBC design was first suggested in 1977[10] and an efficient solar cell was reported in 1984[11].

Recently, in 2014, the highest efficiency in a Si solar cell of 25.6% (144 cm^2: designated area) obtained by a HJ back contact cell was reported[12]. An IBC solar cell with passivated contact exhibited an efficiency of 25.2% (153 cm^2: total area), with the potential to reach 0.26% higher efficiency with designated area, according to their edge loss analysis[13]. Finally, we have reported a 25.1% efficiency top/rear contacted HJ cell (152 cm^2: aperture area) using a Cu electrode[14]. The definitions of the various measurement areas are given in ref. 15.

In this paper, we demonstrate an efficiency over 26% using a large-area (180 cm^2 designated area) c-Si solar cell with an IBC structure combined with an a-Si/c-Si Si HJ, prepared by industrially feasible technologies. With this architecture, by integrating both P^+ and N^+ HJ contacts to the rear side, it is possible to have good optical and passivation properties at the front side of the cell, which receives light. We compare the high-efficiency technologies for Si solar cells in the literature, and discuss the advantages of the technologies used to prepare our record efficiency cell. Finally, a loss analysis pinpoints a path to approach the theoretical conversion efficiency limit[16,17] of Si solar cells, 29.1%.

High conversion efficiency over 26% by the HJ-IBC

Here, we developed a HJ-IBC solar cell with a conversion efficiency of 26.3%, which is a record-breaking efficiency for a Si solar cell. As shown in Fig. 1a, the p-type amorphous Si (p:a-Si) layer and n-type amorphous Si (n:a-Si) layer are patterned to collect holes and electrons, respectively. The front side is covered by an a-Si passivation layer and a dielectric anti-reflection (AR) layer. The incident light generates carriers, which are collected by the patterned a-Si layers and electrodes. The HJ-IBC cell was fabricated using a Czochralski Si wafer with a thickness of 165 μm with resistivity of ~3 Ω cm. The current–voltage (IV) characteristic shown in Fig. 1b was certified by the Fraunhofer Institute for Solar Energy Systems (ISE) with designated area (180 cm^2) measurement

Photovoltaic & Thin Film Device Research Laboratories, Kaneka corporation, 5-1-1 Torikai-Nishi, Settsu, Osaka 566-0072, Japan.
*e-mail: Kunta.yoshikawa@kaneka.co.jp

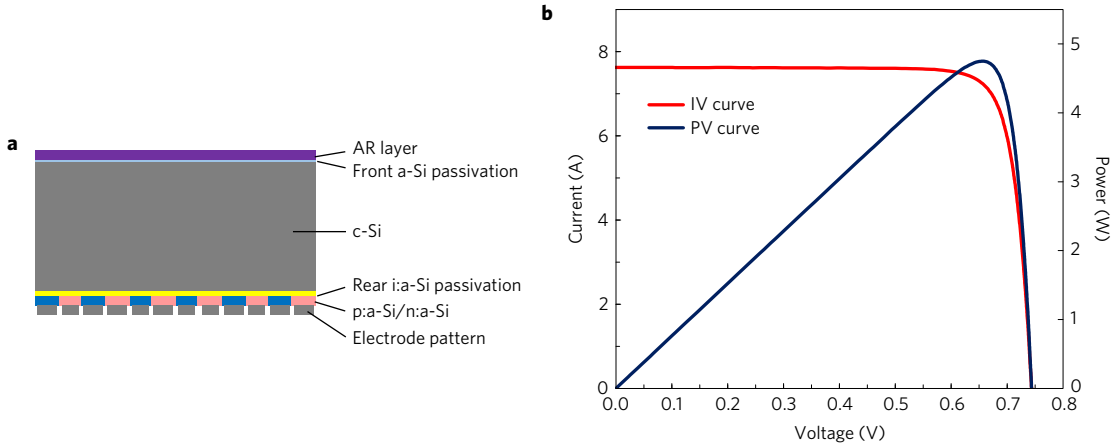

Figure 1 | Schematic image and IV curve of the HJ-IBC cell. a, Cross-section schematic image of the HJ-IBC cell. **b**, Current–voltage (IV) curve and power–voltage (PV) curve of the record HJ-IBC cell (180 cm^2 designated area) with conversion efficiency of 26.3%. The measurement was performed at the Fraunhofer Institute of Solar Energy as a certified measurement by an independent laboratory under standard test conditions. The IV parameters were V_{OC}^{meas} = 0.744 V, J_{SC}^{meas} = 42.3 mA cm^{-2} and FF^{meas} = 83.8% respectively.

Table 1 | Comparison of our HJ-IBC with recent cells from the literature.

Cell type	V_{OC} (V)	J_{SC} (mA cm^{-2})	FF%	Eff%	Area (cm^2)	W (μm)	Article
HJ-IBC	0.744	42.3	83.8	26.3 ± 0.5	180.4 (da)	165	This paper
HJ-IBC	0.740	41.8	82.7	25.6 ± 0.5	143.7 (da)	150	Ref. 12
IBC	0.737	41.3	82.7	25.2 ± 0.5	153.5 (ta)	130	Ref. 13
Top and rear contacted HJ	0.738	40.8	83.5	25.1 ± 0.5	151.9 (ap)	160	Ref. 14
Top and rear contacted HJ	0.750	39.5	83.2	24.7 ± 0.5	101.8 (ta)	100	Ref. 18

Comparison of the IV parameters of the 26.33% HJ-IBC cell and recent high-efficiency cells with HJ architecture[12,14,18] and an IBC cell[13]. The absolute uncertainty of the conversion efficiency and measurement area definition (da, designated area; ap, aperture area; ta, total area) were taken from ref. 15. Designated area: a portion of the cell area from which some cell- or module-contacting components are excluded. Aperture area: the portion of the total cell area that includes all essential components, including active material, busbars, fingers and interconnects. Total area: the total projected area of the cell.

under standard test conditions (25 °C and an illumination of AM1.5 spectrum and 100 mW cm^{-2}). The measured short-circuit current density (J_{SC}) in the IV measurement is consistent to the J_{SC} calculated from the spectral response measurement also performed at the Fraunhofer ISE. The IV measurement was performed with both sweep directions (J_{SC} to open circuit voltage (V_{OC}), V_{OC} to J_{SC}) to take the mean value and there was no hysteresis observed (<0.1%). Importantly, the solar cell was fabricated using an industrially applicable capacitively coupled RF plasma-enhanced chemical vapour deposition (PECVD) deposition tool to form an a-Si layer on a standard Czochralski n-type c-Si wafer.

In Table 1, the IV parameters and the wafer thickness (W) of recent high efficiency works that contain HJ technology in the cell architecture[12,14,18] are compared with the HJ-IBC cell of this work. Although the IBC cell reported in ref. 13 is not an HJ using a a-Si layer, their 'SunPower X-series technology' exhibits similar IV properties to those of our HJ-IBC cells; hence, it is listed for comparison. Due to optically optimized front side architecture, the IBC cells show higher J_{SC} compared with top and rear contacted HJ cells. The fill factor (FF), which is mainly affected by effective lifetime and resistance tends to be higher in top and rear contacted HJ cells compared with IBC cells, while the HJ-IBC cells of this work reached 83.8%. Comparing the V_{OC}, which is affected by effective lifetime, photocurrent density and wafer thickness, the HJ-IBC cell of this work and the top and rear contacted HJ cell reported in ref. 18 seem to have a relatively higher combination of higher effective lifetime with respect to the wafer thickness and/or higher photo/dark current ratio than other devices. Overall, except for the very high V_{OC} (0.750 V) using a thin Si wafer with a thickness of ~100 μm (ref. 18), the IV parameters of the HJ-IBC from this work have shown the highest values.

In the Si solar cell field, because of its long development history and the numbers of players, many types of device structure have been developed aiming for high efficiency. Figure 2 outlines the cross-sectional schematic profiles together with the record efficiency of typical mono-crystalline Si solar cells categorized by type of junction (homo- or heterojunction) and in type of contact (top and rear contacted or IBC). In general, the front side of the substrate has textured pyramid structures with Si (111) surface processed by anisotropic etching of mono-crystalline Si substrate, which is omitted in the Fig. 2.

The HJ technology using a-Si as the passivation layer is known as one of the strongest technologies to obtain high-efficiency Si solar cell by means of reduced carrier recombination loss at the surfaces of Si wafer[12,14,18–22]. Also, the IBC structure is known as the most ideal structure for high-efficiency solar cells by means of reduced optical loss due to the lack of a front side electrode[10,11,13,23].

In general, the HJ cells have a tendency to show a higher open circuit voltage (V_{OC}) of 0.730 ~ 0.750 V compared with that of the homojunction type due to the high-quality passivation and passivated contact structure[12,14,15,19–22]. The core of the HJ technology is to form a very thin hydrogenated a-Si layer on the crystalline Si surface by a PECVD method or hot-wire CVD method.

On the other hand, passivation layers used in homojunction devices such as thermal oxidation or Al_2O_3 passivation can achieve a similar effective lifetime to that of HJ[24]. As these layers are dielectric and do not permit carrier transport, local openings should be made for contacting. However, once such a direct metal

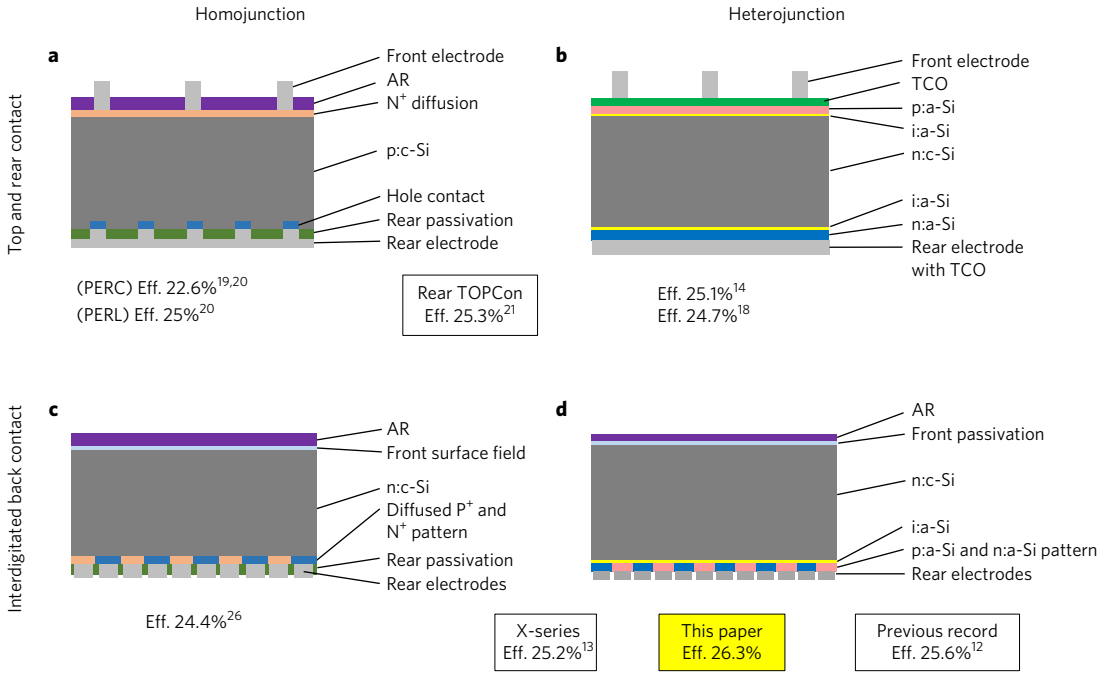

Figure 2 | Schematic images of typical c-Si solar cells and record efficiencies. a, A top/rear contacted homojunction solar cell. The cell architecture that contains a top/rear contacted cell structure that has a diffused region or Al-BSF (back surface field) in the crystalline Si substrate directly contacted by a metal electrode. Passivated emitter and rear cell (PERC)[25,26] and passivated emitter with rear locally diffused (PERL)[26] architecture are categorized here. The architecture reported in ref. 28 has a passivated N^+ contact at the rear side, which is different from this category definition; TOPCon cell efficiency record is also described here. **b**, A top/rear contacted HJ solar cell. The P^+ HJ layer stack (i:a-Si followed by p:a-Si) and N^+ HJ layer stack are formed on the front and rear side of the crystalline Si substrate respectively. On these HJ layer stacks, P^+ and N^+ electrodes including a TCO (transparent conductive oxide) layers are formed. **c**, A homojunction IBC solar cell that has interdigitated P^+ and N^+ diffused regions in the Si substrate directly contacted by hole and electron contacts respectively. **d**, A HJ-IBC cell that has interdigitated P^+ and N^+ HJ layer stacks contacted by P^+ and N^+ electrodes respectively. As the IBC cell reported in ref. 13 is difficult to categorize here, it is described as 'X-series' according their report[13].

contact is formed at the diffused region in the Si substrate, a high recombination velocity at the contact points dominates the entire cell effective lifetime and V_{OC} would be limited to 0.640 $\sim$ 0.71 V (refs 24–27). An efficiency of 25.3% with V_{OC} of 0.718 V was reported in a top and rear contacted solar cell using a homojunction P^+ contact for the front side and a N^+ thin oxide passivated contact (TOPCon) architecture for the rear side of n-type mono-crystalline Si substrate[28]. This cell, which is a hybrid of direct contact and passivated contact, currently has the highest efficiency for a top and rear contacted Si solar cell.

The advantage of the back contact structure is shown in Fig. 2b,c: all of the electrical collection regions and contacts for both holes and electrons are formed at the rear side of the device. The front side of IBC solar cells can be optimized focusing on optical and passivation properties while that of top and rear contacted solar cells requires additionally carrier collection functionality on the front side.

Several groups have worked to develop HJ-IBC solar cells[12,29–35]. In addition to these works, our result strongly indicates that the device structure of HJ-IBC is the optimal structure to achieve high conversion efficiency in the present Si solar cell technology.

Theoretical efficiency limit

There have been many theoretical studies on the conversion efficiency limit of Si solar cells. The calculation of efficiency limit previously carried out in ref. 16 was recently updated in ref. 17. The theoretical limit was calculated considering the intrinsic limitation from the c-Si wafer with no surface or defect-related recombination of photo-generated carriers[16,17]. This theoretical model relies on the assumption of a perfect Lambertian light trapping scheme. As a consequence, the highest theoretical efficiency is predicted to be $\eta^{\mathrm{theo,undoped}}$ = 29.4% for a Si solar cell with a 110-μm-thick undoped Si wafer[17] and IV parameters of $V_{OC}^{\mathrm{theo,undoped}}$ = 0.761 V, $J_{SC}^{\mathrm{theo,undoped}}$ = 43.3 mA cm^{-2} and $FF^{\mathrm{theo,undoped}}$ = 89.3%.

Theoretical efficiency limit for our doped substrate

In a real solar cell, the effective lifetime is also limited by the surface recombination due to surface states and the Shockley–Read–Hall (SRH) recombination due to defects in the Si wafer. To passivate the surface states of c-Si, various passivation techniques have been developed in the photovoltaic field[36]. In real solar cells, it is also difficult to have ideal optical properties (that is, zero reflection at the front side and 100% Lambertian reflection at the rear side) throughout the entire Si device wavelength range, 300–1,200 nm. The optical properties are limited by the choice of the process techniques such as the optical properties of the passivation layers, electrodes and the AR layers[37]. Moreover, there are power losses due to series resistance during the current collection. Series resistance exists in all resistive material along the carrier collection path. Many solutions to reduce the series resistance in different parts in the carrier collection passes have been proposed[38–40], but it is difficult to fabricate a solar cell with a low series resistance with completely undoped Si wafer. Using the substrate thickness and resistivity (165 μm, 3 Ω cm^2) obtained in this work, the theoretical limit becomes η^{theo} = 29.1% (V_{OC}^{theo} = 0.752 V, J_{SC}^{theo} = 43.7 mA cm^{-2}, FF^{theo} = 88.5%) (ref. 17). This is slightly lower than the theoretical limit with optimum substrate selection (undoped, 110 μm). Unless otherwise noted, the theoretical limit value obtained for our substrate parameters is used in this paper.

Loss analysis relative to the theoretical efficiency limit

In this section, we investigate the 9.5% difference between the theoretical limit for the doped substrate of η^{theo} = 29.1% and

the actual efficiency of η^{meas} = 26.3% obtained in our HJ-IBC by examining in detail the device parameters obtained from IV measurements (V_{OC}, J_{SC}, EQE, FF and ideality factor) and discussing recombinations and other loss pathways.

Firstly, for the V_{OC}^{meas} value of 0.744 V, in comparison with the theoretical limit of V_{OC}^{theo} = 0.752 V, there is room to improve 1.1% (8 mV). The difference can be attributed to the lower effective lifetime in the HJ-IBC cell due to the existence of surface and SRH recombination. The V_{OC} difference can also be due to a lower J_{SC}^{meas} compared with J_{SC}^{theo}, but this effect is expected to be smaller than that of lower effective lifetimes.

The J_{SC}^{meas} value of 42.25 mA cm^{-2} is one of the highest values obtained in a c-Si solar cell for a thickness of 165 μm and is 3.4% lower than the theoretical limit J_{sc}^{theo} = 43.7 mA cm^{-2}. To narrow down the origin of this 3.4% J_{SC} loss, external quantum efficiency (EQE) measurements of the HJ-IBC solar cell were performed. In Fig. 3, the EQE spectra (EQE^{theo}) of the HJ-IBC solar cell measured by the Fraunhofer ISE are compared with the calculated ideal EQE (EQE^{theo}) spectra used for the theoretical limit calculation[17]. The integrated current density calculated from the EQE^{meas} is 42.34 mA cm^{-2}, which is consistent with J_{sc}^{meas} from IV measurements, considering the uncertainty of both measurements. The internal quantum efficiency (IQE) spectra of the HJ-IBC cell is calculated using IQE = EQE/(1 − R%), where R% is reflectivity from reflection spectra measured in-house.

The comparison of the EQE^{meas} and EQE^{theo} indicates that ~1.7% loss is coming from the wavelength range of 300 nm to 900 nm, while another ~1.7% loss is from 900 to 1,200 nm. Since the penetration depth of light in most of the short wavelength range (300–900 nm) is shorter than the thickness of the Si wafer, almost all J_{SC} loss in this wavelength range can be related to the front surface of the HJ-IBC cell. This loss in the short wavelength part can be separated into front surface reflection loss of 0.6% and another 1.1% loss such as parasitic absorption most probably in the front a-Si passivation layer and recombination loss at the front surface or bulk recombination during the lateral carrier transport. It should be noted that the uncertainty of the EQE measurement is ~10% in the 300–400 nm range and 2 ~ 3% in the 400–900 nm range; therefore, the detailed quantification is open to question. The J_{SC} loss in the long wavelength range can be separated into small front surface reflection loss (~0.1%) and other main losses (~1.6%) from the rear side such as poor light trapping of the HJ-IBC compared with Lambertian light trapping, parasitic absorption of the a-Si layer and electrodes compared with perfect optics in the theoretical limit and transmission losses. Parasitic absorption can be decreased simply by reducing the thickness or by modifying the optical property of the absorber layer. However, such approaches to improve the optical properties of the cell contain the risk to degrade the electrical properties such as passivation or contact resistivity. The transmission losses are due to the IBC architecture, in which the P^+ and N^+ electrodes must be electrically isolated. In most cases, electrical insulation is achieved by separating the P^+ and N^+ electrodes laterally, and light only partially passes through this separation region. This transmission loss can be reduced by narrowing the separation region or depositing insulating reflection material to this region. We think such insulating reflection material could be, for example, a nanoparticle layer of transparent material in the infrared region such as TiO_2, ZnO and Al_2O_3. The maximum J_{SC} improvement of 0.15 mA cm^{-2} is expected by reducing this transmittance loss.

The cell FF^{meas} of 83.8% is probably one of the highest values observed in Si solar cells; however, it has the largest loss of 5.3% with respect to the theoretical limit FF^{theo} = 88.5% compared with the V_{OC} loss (1.1% loss) and the J_{SC} loss (3.4% loss). Suns-V_{OC} measurements of the HJ-IBC cell were performed in-house to analyse the FF loss. The Suns-V_{OC} pseudo IV curve, constructed from V_{OC} measurements at different incident light intensities (Suns), is unaffected by the voltage drop due to series resistance (R_S) (ref. 41). The pseudo IV curve from Suns-V_{OC} measurements shown in Fig. 4a indicates a diode characteristic free from R_S. The pseudo FF (pFF: FF excluding R_S power loss) of 85.6% and pseudo efficiency (efficiency excluding R_S power loss) of 26.9% are estimated. From the difference between FF^{meas} = 83.8% and pFF = 85.6%, the resistive loss relative to the theoretical limit is estimated to be 2.0% by $(pFF–FF^{meas})/FF^{theo}$ = (85.6% − 83.8%)/88.5%. By fitting the pseudo IV curve to the real IV curve, R_S is estimated to be ~0.32 Ω cm^2, which should be the cause of this 2.0% resistive loss. Another 3.3% loss can be attributed to the lower effective lifetime of the HJ-IBC affected by SRH and surface recombination.

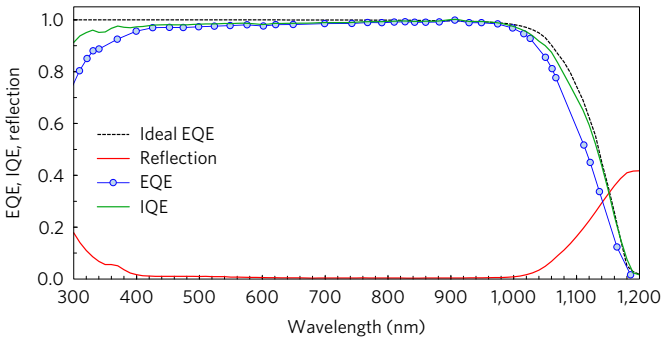

Figure 3 | Quantum efficiency and reflection spectra. External quantum efficiency (EQE^{meas}) measured by the Fraunhofer ISE (blue circles), reflection spectra measured in-house (red line) and internal quantum efficiency (IQE, green line) of the 26.3% HJ-IBC cell. The theoretical limit EQE^{theo} (dotted line) calculated in ref. 18 is shown for comparison. EQE indicates the ratio of electrons provided to the external circuit per photon incident on the device. The EQE^{theo} was calculated for the same wafer thickness as the HJ-IBC cell (165 μm) assuming '100% IQE', 'no front side reflection' and Lambertian light trapping. The free carrier absorption is neglected in this calculation.

To evaluate the impact of additional recombination pathways in the HJ-IBC cell, we calculated the effective lifetime from the HJ-IBC Suns-V_{OC} data, following ref. 41. The equations used to fit the effective lifetime are described in the Methods. Here we use intrinsic lifetime (τ_{intr}) (ref. 42), constant lifetime (τ_{const}) and J_0 to fit the effective lifetime, where τ_{const} includes τ_{SRH} and front surface recombination, and J_0 is the saturation current density from the rear side surface with a doped a-Si layer[43].

Together with τ_{intr} (ref. 42), τ_{const} and J_0 are estimated to be 8.8 ms and 3.0 fA cm^{-2} respectively, which should be the origin of the 3.3% FF loss relative to the theoretical limit.

The ideality factors from the Suns-V_{OC} measurement and modelled curve are shown in Fig. 4b. Both curves peak at ~1.2 around the maximum power point (V = 0.667 V) and decrease at the high voltage region. This is due to the increasing role of Auger recombination, which is expected to lead to an ideality factor of 0.66 in the very high voltage region (>1.0 V). Thus, the ideality factor lower than unity at the high voltage region (>0.7 V) can be attributed to Auger recombination, coupled with a transition from low to high injection level. The difference in the ideality factors between the measured data and the modelled curve at the high voltage region can also be seen in the Suns-V_{OC} plot shown in Fig. 4c.

The V_{OC} of the HJ-IBC above 1 sun illumination is slightly lower (~3 mV at 3 sun illumination) compared with the modelled curve. Such V_{OC} decrease observed at higher intensity can be ascribed either to a higher Auger recombination rate than in the model, or to a voltage decrease due to a partial Schottky contact[41,44], or to the existence of a barrier at the c-Si/a-Si interface[45], or a combination

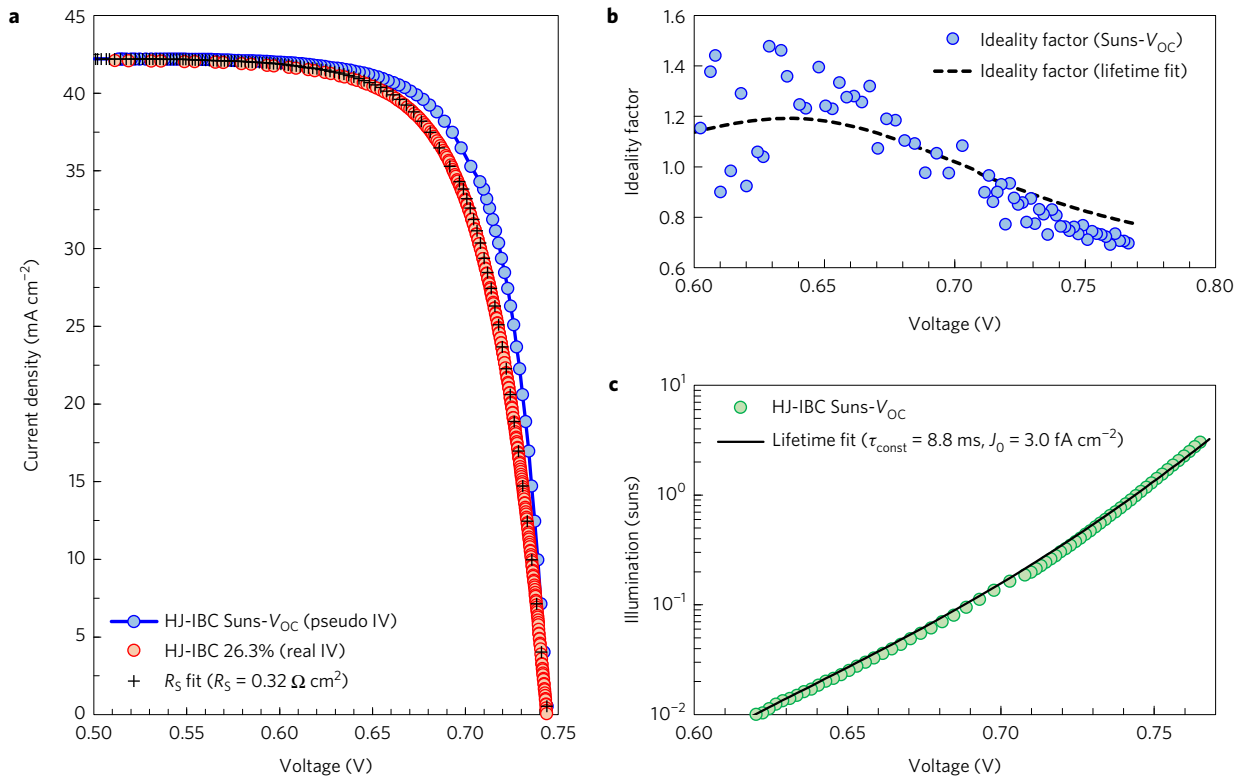

Figure 4 | Extraction of series resistance and ideality factor using Suns-V_{OC}. **a**, Pseudo IV curve (blue circles) from Suns-V_{OC} and the real IV curve (red circles) of the 26.3% HJ-IBC cell. The pseudo IV curve is constructed by a V_{OC}-J_{SC} (suns) plot at different intensity. The illumination intensity is monitored by a calibrated reference cell. The J_{SC} values of Suns-V_{OC} are calibrated using J_{SC}^{meas} = 42.3 mA cm^{-2} from the IV measurement[41]. By fitting the pseudo IV curve to the real IV curve (black crosses), R_S of the HJ-IBC cell is estimated to be 0.32 Ω cm^2. **b**, Ideality factor calculated from the Suns-V_{OC} curve (blue circles) and lifetime fitted curve (dashed line). **c**, The Suns-V_{OC} plot of the HJ-IBC cell (green circles) and lifetime fit using equations (1)–(5) in Methods (solid line).

of these possibilities. To investigate this issue with more accuracy, Suns-V_{OC} measurement at higher illumination (>10 suns) (refs 41,44,45) and detailed analysis of the contact property would be required.

Practical efficiency limit for a highly passivated sample

The practical efficiency limit of the HJ-IBC cell is estimated by applying our best quality HJ passivation. A passivated sample is fabricated using a Si wafer selected from the neighbour position of the same Si ingot as used in the 26.3% HJ-IBC cell to obtain equivalent bulk properties such as resistivity and τ_{SRH}. As shown in the cross-section schematic image in Fig. 5a, the front surface is covered by an a-Si passivation layer followed by a dielectric AR layer, while the rear surface is covered by an i:a-Si passivation layer followed by patterned p:a-Si and n:a-Si layers. The process before passivation is carefully controlled to have substantially identical substrate thickness, surface morphology and bulk properties to those of the HJ-IBC cell. These wafer selection and process controls are designed to exclude the influence of the above factors from the comparison of effective lifetimes between the HJ-IBC cell and the passivated sample.

Figure 5b shows the effective lifetime in the best passivated sample measured by a quasi-steady-state photoconductance method. By modelling the effective lifetime of the passivated sample using the intrinsic lifetime[42], τ_{const} of 14.9 ms and J_0 of 0.9 fA cm^{-2} are estimated respectively, resulting in τ_{extr} of 11.2 ms at the maximum power point.

The implied IV curve shown in Fig. 5c is constructed from this effective lifetime using equations (1) and (2) by applying the J_{SC}^{calc} of 42.4 mA cm^{-2}, which includes the 0.15 mA cm^{-2} improvement expected from a reduced rear side transmittance. The implied efficiency calculated from the effective lifetime of the passivated sample is found to be 27.5%. The modelled lifetime curve is also transformed to a implied IV curve with an implied V_{OC} value of 0.748, implied FF of 86.6% and the same implied efficiency as the passivated sample.

Using the anticipated R_S value of 0.25 Ω cm^2, a FF of 85.3% and an efficiency of η^{pract} = 27.1% can be calculated. We think this reduction of R_S is possible by improving the interface resistance that exists in the rear side architecture. Although this efficiency is derived from the effective lifetime of the passivated sample without electrode contact, we recognize this as the practical limit that could be achieved. Depending on the balance of $\tau_{surface}$ and τ_{SRH}, which is not determined in this study, this practical limit could be pushed to a slightly higher value by wafer selection.

Furthermore, in Fig. 6 the cell efficiency and absolute efficiency losses with respect to the theoretical limit (η^{theo} = 29.1%) (ref. 17) are compared with our HJ-IBC cell result (η^{meas} = 26.3%) and the practical limit (η^{pract} = 27.1%).

In the practical limit case, the optical loss is improved by ~0.1% absolute to the loss in our HJ-IBC cell by reducing the transmittance loss at the rear side, leading to a 0.15 mA cm^{-2} improvement in J_{SC}. Similarly, the extrinsic recombination loss is reduced by ~0.4% relative to our HJ-IBC cell, with τ_{extr} at the maximum power point improved to 11.2 ms (τ_{const} = 14.9 ms, J_0 = 0.9 fA cm^{-2}) in the passivated sample from 5.6 ms (τ_{const} = 8.8 ms, J_0 = 3.0 fA cm^{-2}) in the HJ-IBC.

Finally, the resistive loss in the practical limit case is reduced by 0.1% relative to the HJ-IBC cell by improving the series resistance R_S from 0.32 Ω cm^2 to 0.25 Ω cm^2.

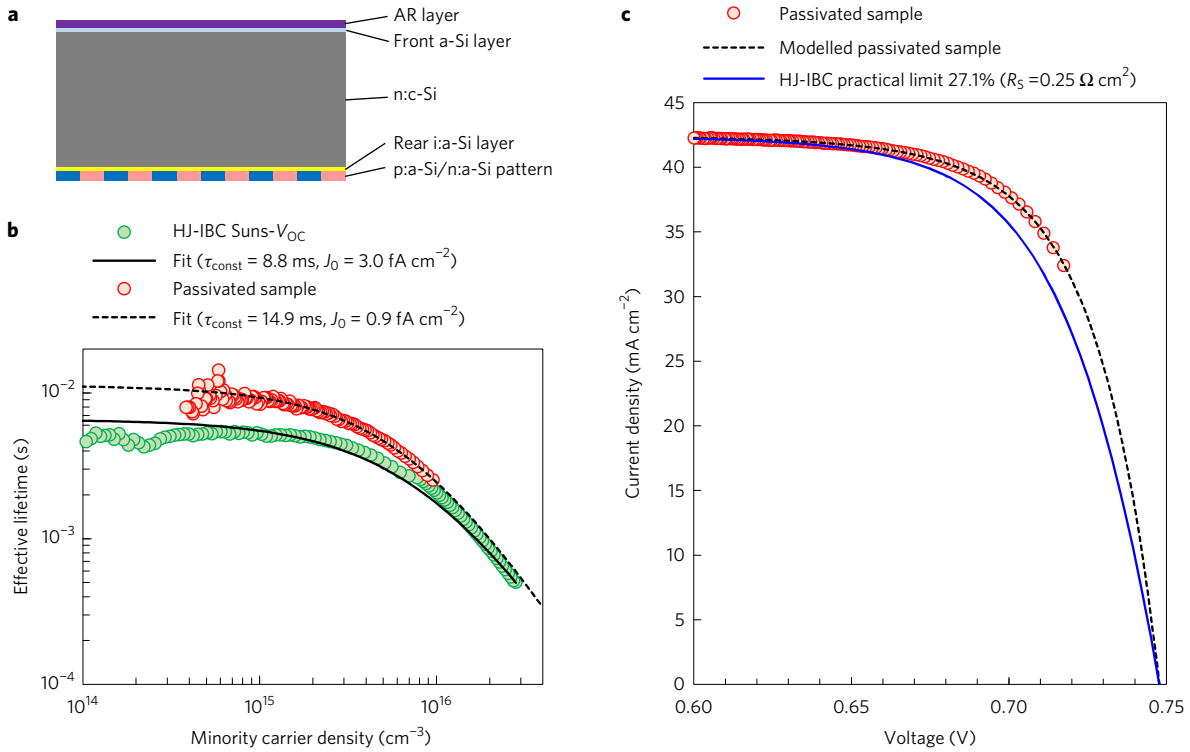

Figure 5 | Effective lifetime and implied IV of the practical efficiency limit. a, Cross-section schematic image of a passivated sample. The front side of the substrate is passivated by a-Si and a dielectric layer (AR layer) while the rear side is passivated by i:a-Si and interdigitated patterned p:a-Si and n:a-Si. **b**, Effective lifetime of the passivated sample (red circles) compared with the HJ-IBC effective lifetime (green circles) from Suns-V_{OC} measurement. The passivated sample is estimated to have τ_{const} of 14.9 ms and J_0 of 0.9 fA cm^{-2} by modelling using t_{intr} from ref. 42 (black dashed line). The HJ-IBC cell is estimated to have τ_{const} of 8.8 ms and J_0 of 3.0 fA cm^{-2} (black solid line). For the calculation, a doping density of $N_D = 1.5 \times 10^{15}$ cm^{-3} and substrate thickness of 165 μm were used for both the HJ-IBC cell and the passivated sample. **c**, The implied IV curve calculated from the effective lifetime of the passivated sample (red circles), modelled lifetime of the passivated sample (black dashed line) and practical limit applying R_S = 0.25 Ω cm^2 (blue solid line).

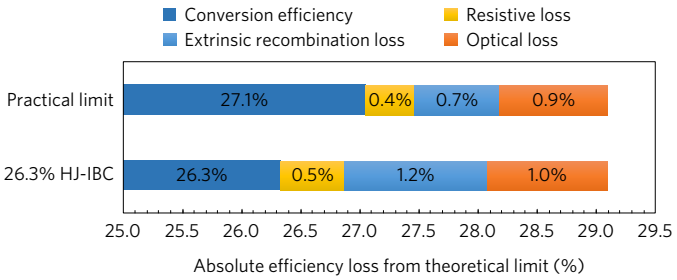

Figure 6 | Summary of loss elements. Summary of loss elements for the 26.3% HJ-IBC cell and the practical limit. The values shown here are absolute conversion efficiency and absolute efficiency loss from the theoretical limit[17]. For both the practical limit and the HJ-IBC cell case, intrinsic and extrinsic recombination is estimated using the intrinsic lifetime equation from ref. 42.

In 2005, a practically achievable efficiency of 26% was estimated, corresponding to an intrinsic efficiency of 26.7% (the intrinsic efficiency neglects resistive loss and lateral transport losses)[46]. It was predicted that IBC cells will closely approach this intrinsic efficiency (26.7%) (ref. 46). Considering the change in standard solar spectrum in 2008[26], this estimation can now be scaled to an intrinsic efficiency of ~27.0% and a practically achievable efficiency of ~26.3% respectively. These scaled values show good agreement with the pseudo efficiency of 26.9% and the efficiency of η^{meas} = 26.3% achieved here by the HJ-IBC cell. Thus, these predictions are demonstrated to be quite correct.

Conclusion

In this paper we have demonstrated a high efficiency of 26.3% by developing the HJ-IBC solar cell by means of high-quality thin-film HJ passivation technology and low-resistance electrodes. The high J_{SC}^{meas}, V_{OC}^{meas} and FF^{meas} was possible by dedicating the front side architecture to collect the light with small current loss, while the rear side architecture was optimized to collect the photo-generated carriers with very low power loss.

Suns-V_{OC}, EQE and reflection measurements were performed on the HJ-IBC cell to characterize the essential elements (effective lifetime, R_S, optical properties) that allowed this record efficiency. By comparison of these measured cell data and the theoretical limit η^{theo} = 29.1% (ref. 17), it became clear that the largest losses in FF are due to an extrinsic lifetime τ_{extr} = 5.6 ms at the maximum power point (τ_{const} = 8.8 ms, J_0 = 3.0 fA cm^{-2}) and to series resistance R_S of 0.32 Ω cm^2. Additionally, we have shown that a passivated sample with the estimated τ_{extr} = 11.2 ms at the maximum power point (τ_{const} = 14.9 ms, J_0 = 0.9 fA cm^{-2}) allows one to expect a practical photoconversion efficiency limit at η^{pract} ~ 27.1% using our device design and fabrication process. We think this practical limit can be approached by maintaining the high-quality HJ passivation during the electrode contact.

In addition, after submission of this paper, we have obtained 26.6% efficiency using the HJ-IBC architecture. This result was certified by Fraunhofer ISE, and this new efficiency is shown in the NREL efficiency chart[7].

Finally, it is noteworthy that the HJ-IBC cell presented here is the first to exceed 26% conversion efficiency. This result confirms the strong potential of silicon photovoltaics and in particular of this

HJ-IBC device architecture to closely approach a photoconversion efficiency of 27%.

Methods

The HJ-IBC solar cell. The HJ-IBC solar cell was fabricated using an n-type Czochralski crystalline 6 inch Si wafer with a size of 239 cm^2, a thickness of about 165 µm, and a resistivity of ~3 Ω cm. The front wafer surface was textured by anisotropic etching to minimize the light reflection. From the weight measurement before the metallization process, we clarify the thickness of the wafer to be 165 µm. Rear side passivation is done by a P^+ HJ layer stack (i:a-Si layer deposition followed by p:a-Si layer deposition) and a N^+ HJ layer stack (i:a-Si layer deposition followed by n-type thin-film Si layer deposition) by using a capacitively coupled RF PECVD tool. The front passivation is done by the a-Si layer followed by the first dielectric AR layer deposition using the same PECVD tool as used for the rear side. Additionally, a second dielectric AR layer is deposited on the first dielectric layer to minimize the reflection at the front surface of the HJ-IBC cell in air. The P^+ and N^+ HJ layer stacks are patterned into an interdigitated design on the rear surface. The rear interdigitated pattern is optimized to minimize the series resistance and the recombination. The electrodes are formed on both p:a-Si and n:a-Si layers to form good ohmic contact. There are no high-temperature (<500°) diffusion nor annealing processes performed in the process flow. The deposition temperature of a-Si was kept under 260°.

The designated area is designed to be a square area of 180 cm^2 that is centred to the wafer centre. The electrodes that collect current from each finger electrode are extended to outside of the wafer and then probed from the front side. Due to this electrode structure that lay outside of the aperture area, the measurement area is defined as the designated area according to the definition in ref. 15.

Passivated sample. The passivated sample is fabricated using a Si wafer selected from the same position of the same Si ingot as used in the HJ-IBC cell to have equal bulk properties such as resistivity and τ_{SRH}. The front surface is covered by an a-Si passivation layer followed by the first dielectric AR layer, while the rear surface is covered by an i:a-Si passivation layer followed by a patterned p:a-Si and n:a-Si layer. The deposition temperature of a-Si was kept under 260°.

The process before passivation is carefully controlled to have substantially identical substrate thickness, surface morphology and bulk properties to that of the HJ-IBC cell. All of the layers were controlled to have similar thickness (<10%) as deposited on the HJ-IBC cell. The rear side interdigitated pattern design of the doped a-Si layers is also the same as the HJ-IBC cell. There are no high-temperature (<500°) diffusion nor annealing processes performed in the process flow.

Lifetime calculation. We calculated the effective lifetime from the HJ-IBC Suns-V_{OC} data, following ref. 41. The relation between the minority carrier density (Δn) and the cell V_{OC} can be calculated by the following formula, where N_D is the doping density of the substrate (=1.5 × 10^{15} cm^{-3}), n_i is the intrinsic carrier density, k is Boltzmann's constant, T is thermodynamic temperature and q is elemental charge[41].

$$\Delta n\,[N_D + \Delta n] = n_i^2 \exp\left(\frac{V_{OC}}{kT/q}\right) \tag{1}$$

The effective lifetime (τ_{eff}) can be directly written as a function of the measured V_{OC} and the corresponding photocurrent density (J_{ph}) by the incident light intensity[41].

$$\tau_{eff} = \frac{n_i^2 \exp\left(\frac{V_{OC}}{kT/q}\right)}{J_{ph}\,[N_D + \Delta n]\,/qW} \tag{2}$$

The intrinsic lifetime (τ_{intr}) from the Si substrate, which contains lifetime components due to Auger recombination and radiative recombination, is calculated using the simplified model (equation (20) in ref. 42). The effective lifetime can be described as the reciprocal sum of the lifetimes from the different recombination mechanisms:

$$\frac{1}{\tau_{eff}} = \frac{1}{\tau_{intr}} + \frac{1}{\tau_{extr}} = \frac{1}{\tau_{intr}} + \frac{1}{\tau_{SRH}} + \frac{1}{\tau_{surface}} \tag{3}$$

where the extrinsic lifetime (τ_{extr}) is the reciprocal sum of τ_{SRH} and $\tau_{surface}$, which can be calculated from equation (3) using the measured τ_{eff} and calculated τ_{intr}.

$\tau_{surface}$ is expressed by following equation (4) where S is the surface recombination velocity of the front surface, W is the thickness of the Si substrate and J_0 is the surface saturation current density of the rear surface. To fit the Suns-V_{OC} effective lifetime curve of the HJ-IBC, which has different surfaces for the front and rear sides, we use both constant terms and injection-dependent terms to characterize the surface recombination[43].

$$\frac{1}{\tau_{surface}} = \frac{S}{W} + J_0 \frac{N_D + \Delta n}{q n_i^2 W} \tag{4}$$

As the low carrier density part (<2.0 × 10^{15} cm^{-3}) of the Suns-V_{OC} lifetime curve is almost constant, we assume τ_{SRH} to be constant. Since we do not have a clear value of τ_{SRH} nor S, both are lumped into a constant lifetime (τ_{const}) and used together with J_0 to characterize the extrinsic lifetime (τ_{extr}).

$$\frac{1}{\tau_{extr}} = \frac{1}{\tau_{SRH}} + \frac{S}{W} + J_0 \frac{N_D + \Delta n}{q n_i^2 W} = \frac{1}{\tau_{const}} + J_0 \frac{N_D + \Delta n}{q n_i^2 W} \tag{5}$$

Data availability. The data that support the plots within this paper and other findings of this study are available from the corresponding author on reasonable request.

Received 31 October 2016; accepted 17 February 2017; published 20 March 2017

References

1. *BP Statistical Review of World Energy 2016* (BP, 2016); https://www.bp.com/content/dam/bp/pdf/energy-economics/statistical-review-2016/bp-statistical-review-of-world-energy-2016-full-report.pdf
2. *World Energy Outlook 2015* (IEA, 2015); http://www.worldenergyoutlook.org/weo2015
3. *Solar Quarterly Market Update—China, United States and Japan to Lead Global Solar Installation in 2016* (Mercom Capital Group, 2016); http://www.solareb2b.it/wp-content/uploads/2016/04/ForecastReports-MercomSolarQuarterlyMarketUpdateApr2016.pdf
4. *2014 Outlook: Let the Second Gold Rush Begin* (Deutsche Bank, 2014); https://www.deutschebank.nl/nl/docs/Solar_-_2014_Outlook_Let_the_Second_Gold_Rush_Begin.pdf
5. *Technology Roadmap for Photovoltaic (ITRPV): 2015 Results Including Maturity Report* (VDMA Photovoltaic Equipment, 2016); http://www.itrpv.net/Reports/Downloads
6. Battaglia, C., Cuevasb, A. & Wolf, S. D. High efficiency crystalline silicon solar cells: status and perspectives. *Energy Environ. Sci.* **9**, 1552–1576 (2016).
7. *Best Research-Cell Efficiencies* (NREL, 2016); http://www.nrel.gov/pv/assets/images/efficiency-chart.png
8. Green, M. A., Emery, K., Hishikawa, Y., Warta, W. & Dunlop, E. D. Solar cell efficiency tables (version 48). *Prog. Photovolt. Res. Appl.* **24**, 905–913 (2016).
9. Taguchi, M. *et al.* HIT cells: high efficiency crystalline Si cells with novel structure. *Prog. Photovolt.* **8**, 492–502 (2000).
10. Lammert, M. D. & Schwartz, R. J. The interdigitated back contact solar cell: a silicon solar cell for use inconcentrated sunlight. *IEEE Trans. Electron Devices* **24**, 337–341 (1977).
11. Swanson, R. M. *et al.* Point-contact silicon solar cells. *IEEE Trans. Electron Devices* **31**, 661–664 (2005).
12. Masuko, K. *et al.* Achievement of more than 25% conversion efficiency with crystalline silicon heterojunction solar cell. *IEEE J. Photovolt.* **4**, 1433–1435 (2014).
13. Smith, D. D. *et al.* Silicon solar cells with total area efficiency above 25%. In *2016 IEEE 43rd Photovoltaic Spec. Conf.* 3351–3355 (IEEE, 2016).
14. Adachi, D., Hernandez, J. L. & Yamamoto, K. Impact of carrier recombination on fill factor for large area heterojunction crystalline Si solar cell with 25.1% efficiency. *Appl. Phys. Lett.* **107**, 233506 (2015).
15. Green, M. A., Emery, K., Hishikawa, Y., Warta, D. & Dunlop, E. D. Solar cell efficiency tables (version 39). *Prog. Photovolt. Res. Appl.* **20**, 12–20 (2012).
16. Kerr, M. J., Cuevas, A. & Campbel, P. Limiting efficiency of crystalline silicon solar cells due to Coulomb-enhanced Auger recombination. *Prog. Photovolt. Res. Appl.* **11**, 97–104 (2003).
17. Richter, A., Hermle, M. & Glunz, S. W. Reassessment of the limiting efficiency for crystalline silicon solar cells. *IEEE J. Photovolt.* **3**, 1184–1191 (2013).
18. Taguchi, M. *et al.* 24.7% record efficiency HIT solar cell on thin silicon wafer. *IEEE J. Photovolt.* **4**, 96–99 (2014).
19. Hernandez, J. L. *et al.* High efficiency silver-free heterojunction silicon solar cell. *Jpn. J. Appl. Phys.* **51**, 10NB04 (2012).
20. Hernandez, J. L. High efficiency copper electroplated heterojunction solar cells. In *Proc. 27th EUPVSEC* 655–656 (WIP, 2012).
21. Hernandez, J. L. *et al.* High efficiency copper electroplated heterojunction solar cells and modules—The path towards 25% cell efficiency. In *Proc. 28th EUPVSEC* 741–743 (WIP, 2014).
22. Wolf, S. D., Descoeudres, A., Holman, Z. C. & Ballif, C. High efficiency silicon heterojunction solar cells: a review. *Green* **2**, 7–24 (2012).

23. Franklin, E. *et al.* Design, fabrication and characterisation of a 24.4% efficient interdigitated back contact solar cell. *Prog. Photovolt. Res. Appl.* **24**, 411–427 (2014).
24. Dingemans, G. & Kessels, W. M. M. Status and prospects of Al_2O_3-based surface passivation schemes for silicon solar cells. *J. Vac. Sci. Technol. A* **30**, 040802 (2012).
25. Green, M. A. The Passivated Emitter and Rear Cell (PERC): from conception to mass production. *Sol. Energy Mater. Sol. Cells* **143**, 190 (2015).
26. Green, M. A. The path to 25% silicon solar cell efficiency: history of silicon cell evolution. *Prog. Photovolt. Res. Appl.* **17**, 183–189 (2009).
27. Zhang, S. *et al.* 335 watt world record p-type mono-crystalline module with 20.6% efficient PERC solar cells. *IEEE J. Photovolt.* **6**, 145–152 (2016).
28. Richter, A. *et al.* Silicon solar cells with full-area passivated rear contacts: influence of wafer resistivity on device performance on a 25% efficiency level. In *26th PVSEC* (2016); http://pvsec-26.com/dr-armin-richter
29. Harrisona, S. *et al.* Back contact heterojunction solar cells patterned by laser ablation. *Energy Procedia* **92**, 730–737 (2016).
30. Desrues, T., De Vecchi, S., D'Alonzo, G., Muñoz, D. & Ribeyron, P.-J. Influence of the emitter coverage on interdigitated back contact (IBC) silicon hetero-junction (SHJ) solar cells. In *Proc. 40th IEEE Photovoltaic Spec. Conf.* 857–886 (IEEE, 2014).
31. Lee, S. Y. *et al.* Analysis of a-Si:H/TCO contact resistance for the Si heterojunction back-contact solar cell. *Sol. Energy Mater. Sol. Cells* **120**, 412–416 (2014).
32. Tomasi, A. *et al.* Backcontacted silicon heterojunction solar cells with efficiency > 21%. *IEEE J. Photovolt.* **4**, 1046–1054 (2014).
33. Mingirulli, N. *et al.* Efficient interdigitated back-contacted silicon heterojunction solar cells. *Phys. Status Solidi* **5**, 159–161 (2011).
34. Nakamura, J. *et al.* Development of heterojunction back contact Si solar cells. *IEEE J. Photovolt.* **4**, 1491–1495 (2014).
35. Salomon, B. P. *et al.* Back-contacted silicon heterojunction solar cells: optical-loss analysis and mitigation. *IEEE J. Photovolt.* **5**, 1293–1303 (2015).
36. Aberle, A. G. Surface passivation of crystalline silicon solar cells: a review. *Prog. Photovolt.* **8**, 473–487 (2000).
37. Wang, E. Y., Yu, F. T. S., Sims, V. L., Brandhorst, E. W. & Broder, J. D. Optimum design of anti-reflection coating for silicon solar cells. In *10th IEEE Photovoltaic Spec. Conf.* 168–171 (IEEE, 1973).
38. Fields, J. D. *et al.* The formation mechanism for printed silver-contacts for silicon solar cells. *Nat. Commun.* **7**, 11143 (2016).
39. Zhang, X., Wan, Y., Bullock, J., Allen, T. & Cuevas, A. Low resistance Ohmic contact to p-type crystalline silicon via nitrogen-doped copper oxide films. *Appl. Phys. Lett.* **109**, 052102 (2016).
40. Frühaufa, F., Sayadb, Y. & Breitensteina, O. Description of the local series resistance of real solar cells by separate horizontal and vertical components. *Sol. Energy Mater. Sol. Cells* **154**, 23–34 (2016).
41. Sinton, R. A. & Cuevas, A. A quasi-steady-state open-circuit voltage method for solar cell characterization. In *16th Eur. Photovoltaic Solar Energy Conf.* 1152–1155 (WIP-Renewable Energies, 2000).
42. Richter, A., Glunz, S. W., Werner, F., Schmidt, J. & Cuevas, A. Improved quantitative description of Auger recombination in crystalline silicon. *Phys. Rev. B* **86**, 165202 (2012).
43. Cuevas, A. & Macdonald, D. Measuring and interpreting the lifetime of silicon wafers. *Sol. Energy* **76**, 255–262 (2004).
44. Glunz, S. W., Nekarda, J., Mackel, H. & Cuevas, A. Analyzing back contacts of silicon solar cells by Suns-Voc-measurements at high illumination densities. In *22nd Eur. Photovoltaic Solar Energy Conf.* 849–853 (WIP-Renewable Energies, 2007).
45. Chavali, R. V. K. *et al.* A generalized theory explains the anomalous Suns–Voc response of Si heterojunction solar cells. *IEEE J. Photovolt.* **7**, 169–176 (2016).
46. Swanson, A. Approaching the 29% limit efficiency of silicon solar cells. In *Proc. 31th PVSC, Colorado Springs* 889–895 (Drupal, 2005).

Acknowledgements

This work was supported in part by the New Energy and Industrial Technology Development Organization (NEDO) under the Ministry of Economy, Trade and Industry of Japan.

Author contributions

K.Yoshikawa designed the experiments and analysed the data. D.A. and K.Yamamoto supervised the study. K.Yoshikawa., H.K., W.Y., T.I., K.K., K.N., T.U. and M.K. contributed to development of the HJ-IBC cell, optimization of optical properties, passivation quality and resistivity. K.Yoshikawa, D.A. and K.Yamamoto wrote the manuscript. All authors discussed the results and commented on the manuscript.

Additional information

Reprints and permissions information is available at www.nature.com/reprints.

Correspondence and requests for materials should be addressed to K.Yoshikawa
How to cite this article: Yoshikawa, K. *et al.* Silicon heterojunction solar cell with interdigitated back contacts for a photoconversion efficiency over 26%. *Nat. Energy* **2**, 17032 (2017).

Publisher's note: Springer Nature remains neutral with regard to jurisdictional claims in published maps and institutional affiliations.

Competing interests

The authors are employees of Kaneka Corporation.